A method of downscaling temperature maps based on analytical hillshading for use in species distribution modelling

Á.M. Felicísimo Pérez & M.Á. Martín-Tardío

Taylor & Francis
Taylor & Francis Group

REVIEW ARTICLE

Check for updates

A method of downscaling temperature maps based on analytical hillshading for use in species distribution modelling

Á.M. Felicísimo Pérez [ID][a] and M.Á. Martín-Tardío [ID][b]

[a]Department of Graphic Expression, University of Extremadura, Mérida, Spain; [b]Department of Computing and Telematics System Engineering, University of Extremadura, Mérida, Spain

ABSTRACT

Climate maps have been widely used for the construction of species distribution models. These maps derive from interpolation of data collected by meteorological stations. The sparse distribution of stations generates maps with coarse spatial resolution that are unable to detect microclimates or areas that can serve as plant or animal refuges. This work proposes a method for downscaling temperature maps using the solar radiation falling upon hillsides as predictor for the influence of relief on local variability. Solar irradiance is estimated from a digital elevation model of the study area using a routine based on analytical hillshading. Some examples of downscaling from 1 km to 25 m spatial resolution are shown. The results are compared with the surface temperature maps from Landsat 8 satellite imagery.

Introduction

Climatic cartography has traditionally involved generating maps by means of data interpolation from scattered meteorological station observations. This method has numerous well-known problems, such as the sparse distribution of data, the poor representation of high elevations, and the nonrepresentative distribution over a given terrain. Spatial resolution from such interpolation does not surpass 1 km in the best case and is frequently limited to 10 km or more.

Climate maps have been widely used for the construction of species distribution models (SDM). For example, Worldclim datasets are used in hundreds of studies due to their free availability and worldwide coverage. Hijmans, Cameron, Parra, Jones, and Jarvis (2005) developed interpolated climate surfaces for global land areas (excluding Antarctica) at a spatial resolution of 30 arc s. Worldclim datasets incorporate a spatial resolution of 1 km^2, but this value is obtained by means of interpolation procedures from sparse data and does not represent the real climate variability and complexity of given terrains, especially in mountainous areas. As a consequence, although Worldclim and similar data are very valuable sources of information, they remain problematic in certain aspects and therefore can be useful at continental scales but cannot detect local variability. Beier, Signell, Luttman, and DeGaetano (2012) analyzed two 4 km gridded

historical climate (GHC) products to produce high-resolution temperature trend maps for the US Northeast from 1980 to 2009, and compared outputs between products and with an independent climate record. Trend maps resulting were highly heterogeneous, with local-scale anomalies persistent across months. The comparison between trend maps and GHC products show some large local-scale disparities at the high-altitude areas and along coastlines. The availability of high resolution climate maps would be considerably important for conducting local or microhabitat studies, i.e. studies on the influence of climate change on the distribution of species that can find suitable microclimates as refugia. For example, Meineri and Hylander (2016) developed three sets of large-domain (450,000 km^2), fine-grain (50 m) temperature grids accounting for different levels of topographic complexity, using climate stations and topographic data. Using these fine-grain grids and the Worldclim data, they fitted SDMs for 78 alpine species over Sweden, and assessed underestimations of local extinction and area of microrefugia.

In some countries such as Spain, the problem of data inadequacy has worsened over time due to a significant reduction in the number of climate stations (Felicísimo, Muñoz, Villalba, & Mateo, 2011), which correspondingly reduces the quality of even conventional maps. Consequently, other solutions must be

tested. The most common approach to solve this problem involves the use of downscaling procedures. Downscaling refers to procedures that attempt to use information known at coarse scales to estimate the corresponding values at more detailed scales. There are two main approaches to downscaling climate data: dynamical and statistical (Benestad, Hanssen-Bauer, & Chen, 2008; Trzaska & Schnarr, 2014). Dynamical downscaling applies climate models based on physical principles to reproduce local climate over a finer grid by solving equations of motion and thermodynamics. On the other hand, statistical downscaling establishes empirical relationships between local climate dependent variables and a set of known independent variables or predictors. Within these two approaches, there are numerous procedures proposed: dynamical procedures (Gerelchuluun & Ahn, 2014), probabilistic procedures (Caillouet, Vidal, Sauquet, & Graff, 2016), multiple regression (Landgraf, Matulla, & Haimberger, 2015), neural networks (Coulibaly, Dibike, & Anctil, 2005), support vector machines (Duhan & Pandey, 2015), regression trees (Gerlitz, 2015), etc.

In this work, we propose a method for downscaling temperature maps using the solar radiation falling upon hillsides as predictor or covariable. This variable can be estimated from the topography or digital elevation model (DEM) of the study area. Data such as the latitude of the study area and the day are also required for the simulation. The major advantage of the method is that it does not need external data other than the DEM. It also adapts to the time of year and is particularly suitable for mountainous areas and the generation of change scenarios using only temperature maps (specific to the model and climate scenario) and the DEM.

The study area (Figure 1) is characterized by strong altitudinal temperature gradients and large heterogeneity in local temperature patterns due to the rugged topography and the greatly differing exposure to solar radiation (Figure 2). The main geological structure is a fault in the NE–SW direction that forms the Jerte Valley (Extremadura Region). We have downscaled a set of 24 monthly temperature maps (12 of the maximum temperatures and 12 of the minimum temperatures) corresponding to this mountainous zone. The procedure calculates the solar trajectory over the horizon to estimate exposure to solar energy. Both relief patterns and solar energy are used to build a model of the local temperature patterns.

As expected, topography has been used as a covariable in several downscaling approaches. Fridley (2009) demonstrate that ground-level temperature regimes in Great Smoky Mountains National Park (Tennessee and North Carolina) vary considerably over fine spatial scales and are only partially linked to synoptic weather patterns and environmental lapse rates. Using a sensor network deployed across two watersheds in 2005–2006, and linking the sensor array data to 10 regional
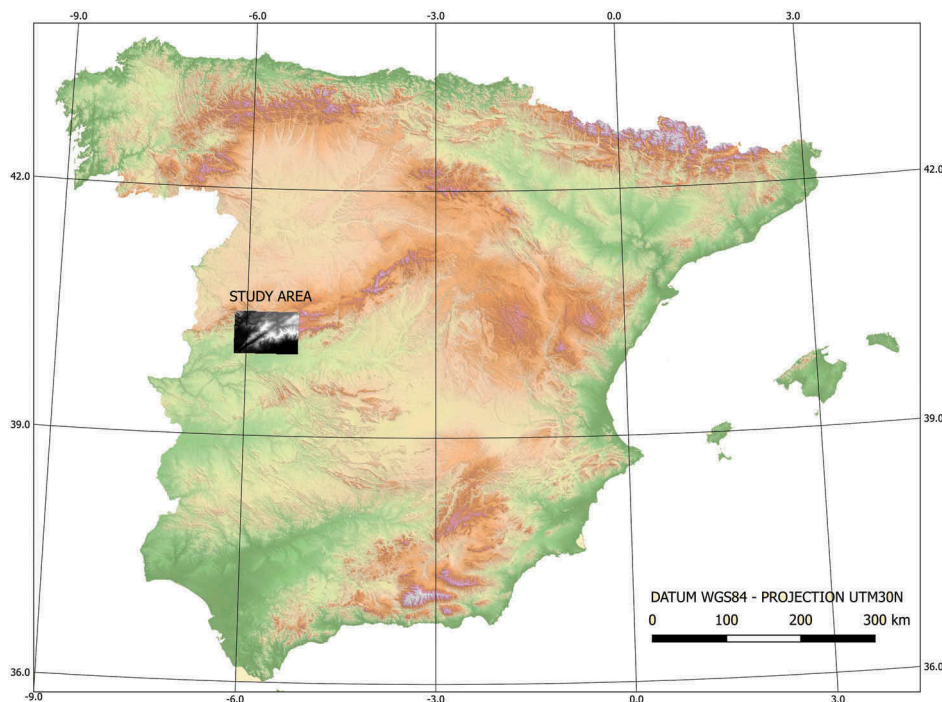

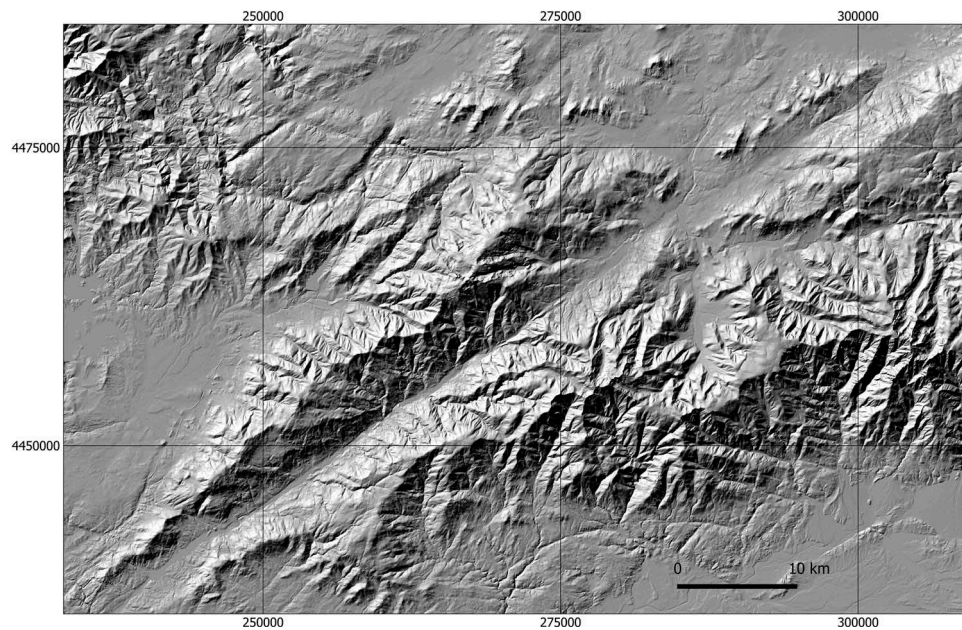**Figure 1.** Study area situation map.

Figure 2. Analytical hillshading of the study area reveals its mountainous relief.

weather stations and topographic variables describing site radiation load and moisture content, multilevel spatial models of 30 m resolution were constructed to map daily temperatures across the 2090 km^2 park.

Feidas et al. (2014) presents a methodology for modeling and mapping the seasonal and annual air temperature and precipitation climate over Greece using several topographical and geographical parameters. Data series of air temperature and precipitation from 84 weather stations distributed evenly over Greece are used along with a set of topographical and geographical parameters extracted with GIS methods from a DEM. Normalized difference vegetation index obtained from moderate resolution imaging spectro-radiometer (MODIS) Aqua satellite data is also used as a geographical parameter.

Slavich, Warton, Ashcroft, Gollan, and Ramp (2014) analyzed the reasons why "topoclimate" mapping methodologies improve on macroclimatic variables in modeling the distribution of biodiversity, and the implications for climate change projections. In Greater Hunter Valley region (60,000 km^2), New South Wales (Australia), they fitted generalized linear models to 295 species of grasses and ferns at fine resolutions (<50 m^2) using: (a) macroclimatic variables, interpolated from weather station data using altitude and location only, (b) topoclimatic variables, interpolated from field measurements using additional climate-forcing factors such as topography and canopy cover, and (c) both topoclimatic and macroclimatic variables. However, the topography variable does not appear to have been used as proposed in this work.

Material and methods

Figure 3 shows the flowchart of the proposed method for downscaling temperature maps.

Study area

The study area covers a mountainous zone of SW Spain (Figure 1), for which the main characteristics are as follows:

- Boundary coordinates (Datum WGS84, projection UTM, zone 30): X_{min} = 227,587, X_{max} = 315,012, Y_{min} = 4,429,787, Y_{max} = 4,488,412.
- Minimum and maximum height values: 235 and 2578 m; mean height: 900 m.
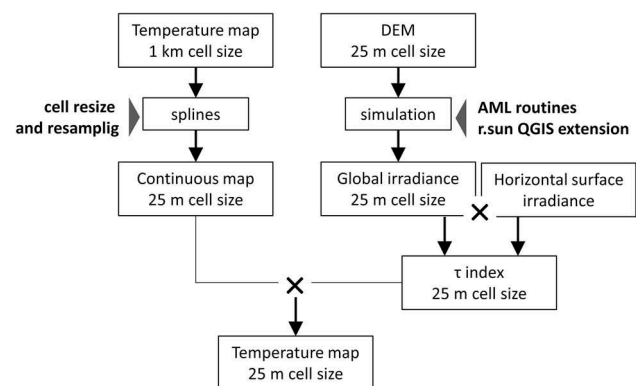- Mean latitude: 41° N.

Figure 3. Flowchart of the proposed method for downscaling temperature maps.

Digital elevation model

The DEM was downloaded from the data web of the Spanish official National Centre for Geographic Information (CNIG, http://centrodedescargas.cnig.es/). Nine DEM sheets were downloaded and joined; the result is a raster DEM of 2345 rows, 3497 columns, and a 25-m cell size. Some border cells were clipped to obtain a rectangle approximately 88 × 59 km in area. Metadata of the DEM ensures a root mean square error <2 m for the height values.

Climate data

We developed climate maps several years ago in the context of a national project for climate change modeling of the Iberian Peninsula (Felicísimo et al., 2011). The maps were generated using data from meteorological recordings using kriging for the interpolation. Later, empirically calculated monthly height gradients were added for better representation of the high-altitude areas without meteorological records. A large set of maps (monthly from 1950 to 2007) with a 1-km cell size was generated for the variables of minimum temperature, maximum temperature, and precipitation (Figure 4). In this work, we use the mean values of the minimum and maximum temperatures for the reference period 1961–1990. We emphasize that the map time range is not relevant for explanation or application of the downscaling method.

Software and code

We performed the analysis using the GIS software ArcInfo (ESRI Inc.). ArcInfo is an old GIS but exhibits strong performance in massive calculations and is suitable for running some essential parts of the code. All the routines have been programmed in arc macro language (AML), the specific programming language used by ArcInfo. We recognize that this decision is controversial because AML is an obsolete language. We chose it because it was comfortable for us but we understand that it is not in common use. The simplest procedure to replicate this work is to use QGIS or GRASS and the r.sun routines. Specifically, r.sun computes direct (beam), diffuse, and reflected solar irradiation raster maps for given day, latitude, surface, and atmospheric conditions. The workflow with QGIS or GRASS is the same as with Arcinfo.

Methods: general workflow

Solar radiation estimation

The procedure based on the hypothesis that solar energy is a main factor driving local temperature variability. Obviously, under a given environment, hillsides facing the sun have higher temperatures than ones in the shade. The aim herein is to estimate a *topographic index* derived from the incident solar radiation that can be applied to each DEM cell with size 25 m to increase or decrease the temperature of the corresponding temperature map cell with size 1 km.
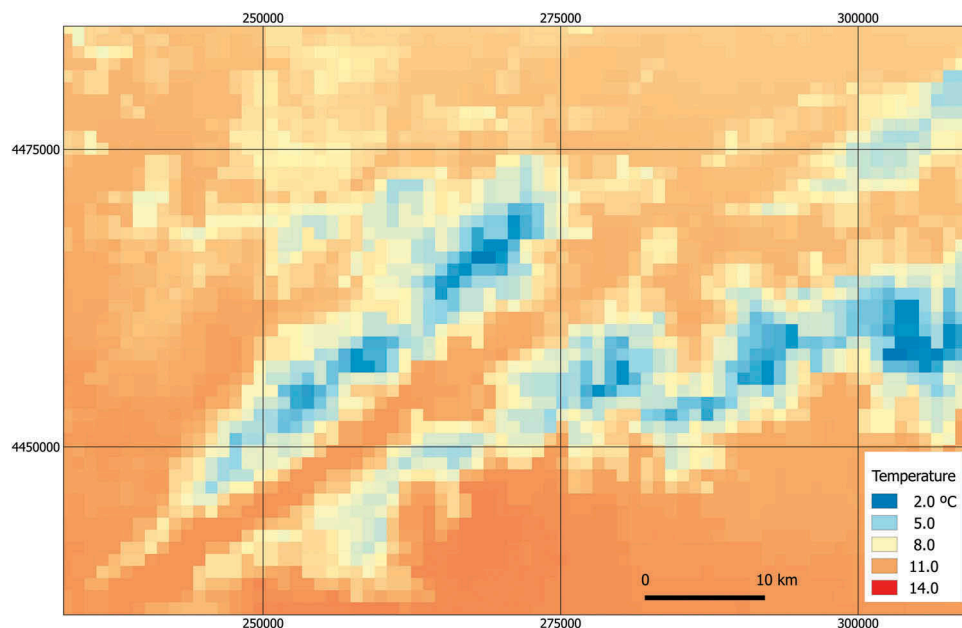

Figure 4. Example of a temperature map (cell size 1 km) of the study area. The variable is the mean maximum temperature in January for the period 1961–1990. The more conspicuous temperature patterns are due to the altitudinal gradient.

The first step is to estimate the potential solar irradiation over each 25 m DEM cell. This variable was estimated using the equations of Kumar, Skidmore, and Knowles (1997), which were programmed by N. E. Zimmermann in AML (http://www.wsl.ch/staff/niklaus.zimmermann/progs.html) but as discussed earlier, the r.sun module can also be used in GRASS and QGIS systems. The AML routines (shortwavc.aml and diffuse.aml) are freely available on the programmer's web page and calculate direct and diffuse solar radiation. The inputs in both cases (AML and r.sun) are DEM, latitude (°), Julian day (from 1 to 365), and time interval (min) for the integration of a solar path. The routines determine how often sun position is calculated during a day as a function of the time interval. The incidence angle of the solar radiation vector over each DEM cell is calculated for each solar position taking into account the terrain slope and orientation and the potential overshadowing caused by adjacent terrain. The result is output in kJ/(m^2 · day) as a gridded map of potential solar radiation values whose spatial resolution is the same as that of the DEM used. Total solar radiation is the sum of the direct and diffuse components, and the procedure is repeated for each month of the year. At this point, it may be emphasized that the accuracy of the energy estimation is not substantially important; rather, the relative relations between the areas differently exposed are useful.

Topographic index τ calculation

Mamassis, Efstratiadis, and Apostolidou (2012) and Page (1986) examined the effects of topography on radiation, at multiple spatiotemporal scales, using suitable geometric methods for the direct and diffuse components. As a result, it is concluded that solar radiation, direct and diffuse, is affected by surface characteristics, such as slope, aspect, altitude, and shading.

The following step involves the estimation of the topographic index (symbolized as τ) from the previously estimated solar radiation. The rationale for this estimation is that the τ values will indicate how much the temperature of each cell should be modified based on its exposure to solar radiation. For example, if τ = 0.85, the procedure for the cell is to multiply the general 1 km^2 temperature value for this index by 0.85, resulting in a topographically corrected value; i.e. 20.0° C × 0.85 = 17.0°C. This example would correspond to a cell facing north and/or overshadowed by the adjacent relief. The estimation of topographic indexes from solar radiation has been performed by applying the directly proportional relationship between energy E radiated per unit surface area of a black body across all wavelengths per unit time and the fourth power of the black body's thermodynamic temperature T: $E = \sigma \cdot T^4$, where σ is the Stefan–Boltzmann constant. This equation shows how a relationship between energy and temperature can estimate τ values. The procedure is as follows:

- The solar radiation models are transformed by applying the fourth root of the energy values.
- The fourth root of the mean irradiance for the 1 km cell area is also calculated.
- The topographic index τ for each cell is calculated as the ratio between its fourth root value and the mean value of the 1 km cell area.

All steps are performed by means of GIS map algebra operations, and the result is a set of 12 topographic index maps, one for each month of the year.

Applying the topographic index

At this stage of the workflow, it is necessary to apply the topographic indexes to the temperature maps. Since these maps have a spatial resolution of 1 km, it is necessary to reduce the cell size to 25 m to make it compatible with the topographic index grids. We performed this procedure by means of spline interpolations, using the centers of each 1 km cell as data points. The result is a set of maps with the same information as the originals but for which the pixellation has disappeared, and transitions between cells are continuous. The last step is to multiply the two map sets (temperature and topographic indexes) to obtain the downscaled temperature maps.

Testing the maps

A suitable method for testing the map values calculated herein is to deploy a sensor network for *in situ* measurement of temperature. Obviously, a huge number of sensors would be necessary to ensure complete coverage of the environmental variability. This procedure is not within our capacity at this time, and alternative less exhaustive evidence is therefore sought. An alternative test is to calculate the correlation between the downscaled maps and temperature maps derived from satellite thermal images of the same area. We use a Landsat 8 image downloaded by means of the USGS Global Visualization Viewer (GloVis) corresponding to path 202 and row 32; the dates are 14 July 2015, 12 August 2014, 18 September 2016, 31 October 2014, and 15 December 2013 (USGS, 2016).

Our hypothesis is that if the downscaling method is accurate, temperatures from the downscaled map will be significantly correlated with corresponding temperatures derived from the thermal satellite bands. Temperatures
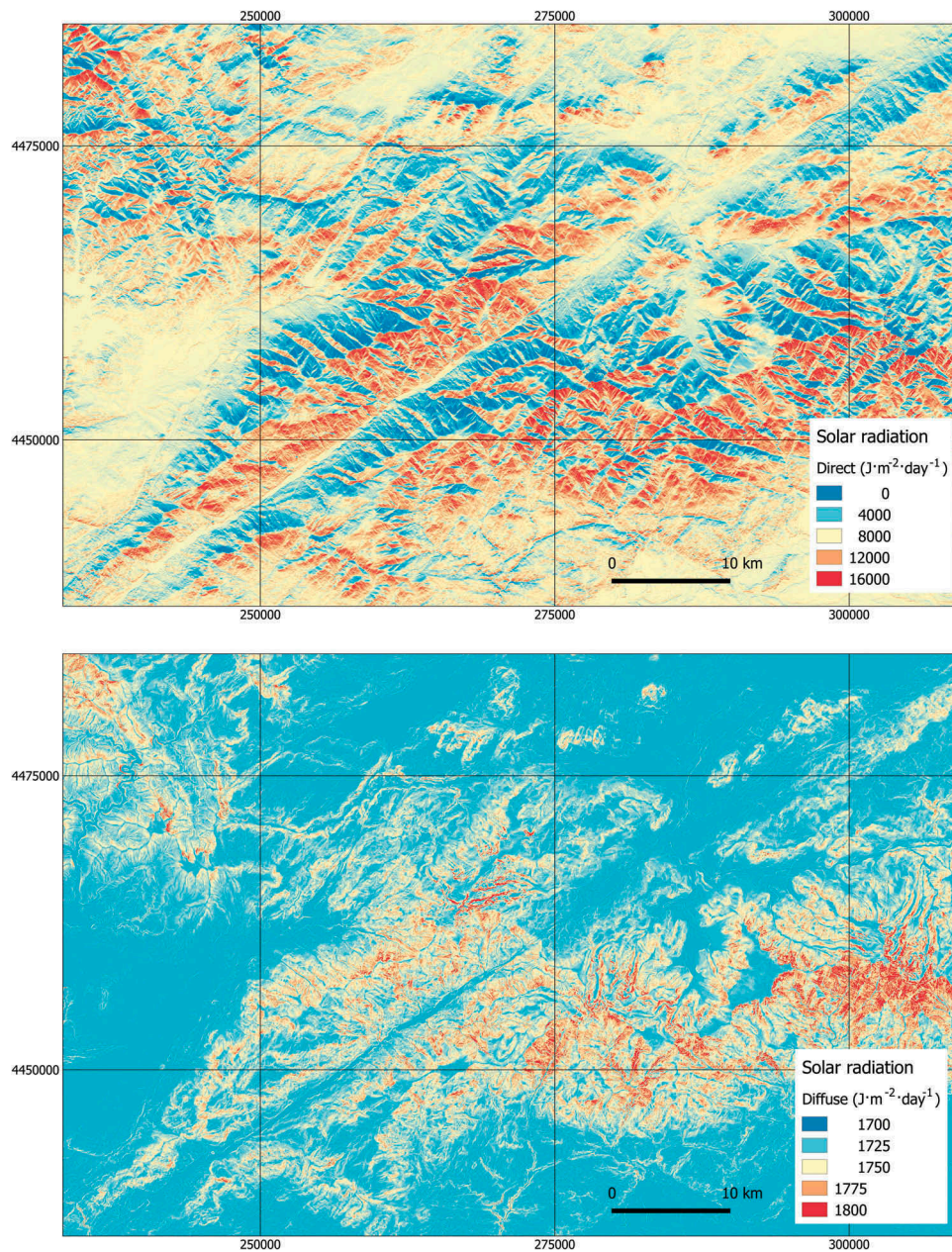
Figure 5. Solar direct (above) and diffuse (below) radiation maps corresponding to January (Julian day 15).

derived from satellite data represent only a snapshot of the monthly temperatures, but the relief-driven pattern must be similar if the proposed model is adequate. The method to estimate temperature values from Landsat 8 imagery is described in "Using the USGS Landsat 8 Product" from USGS web pages (https://landsat.usgs.gov/using-usgs-landsat-8-product).

diffuse radiation (see subsection "Solar radiation estimation") for each month of the year, with day 15 of each month as the reference date. The days as Julian dates are 15, 43, 74, 104, 135, 165, 196, 227, 257, 288, 318, and 349. The time interval was 20 min. As an example, Figure 5 shows the direct and diffuse solar radiation for day 15.

Results

Solar radiation maps

Twenty-four maps of solar radiation were calculated by means of Zimmermann AML routines using direct and

Topographic index

From the total solar radiation estimations and as a function of the solar radiation over a horizontal surface, we calculated a set of topographic indexes, one for
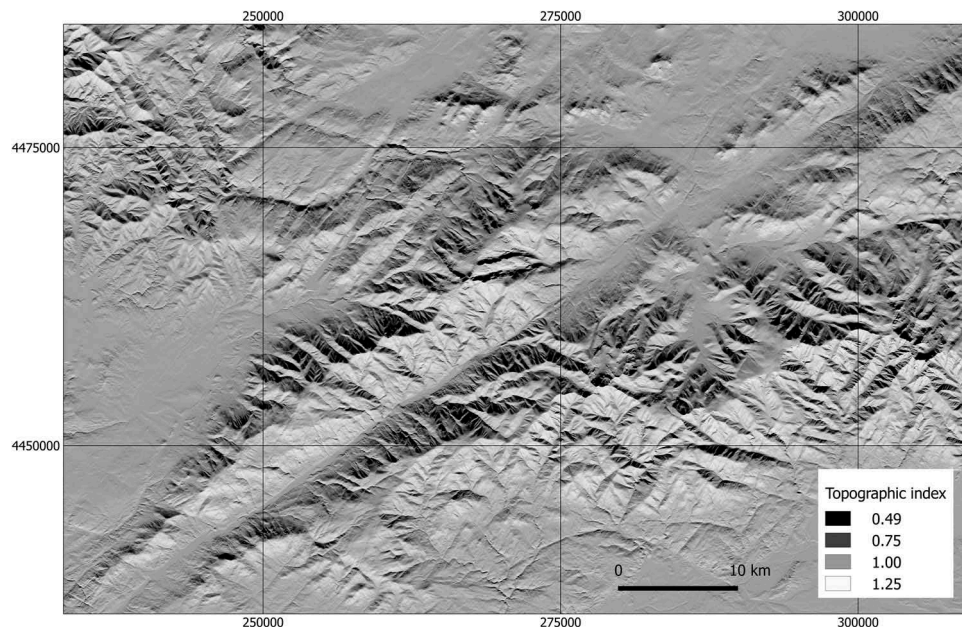
Figure 6. Topographic indexes corresponding to January (Julian day 15). White and light gray tones represent τ > 1 (oriented to the south), and dark gray tones represent τ < 1 (shaded or oriented to the north).
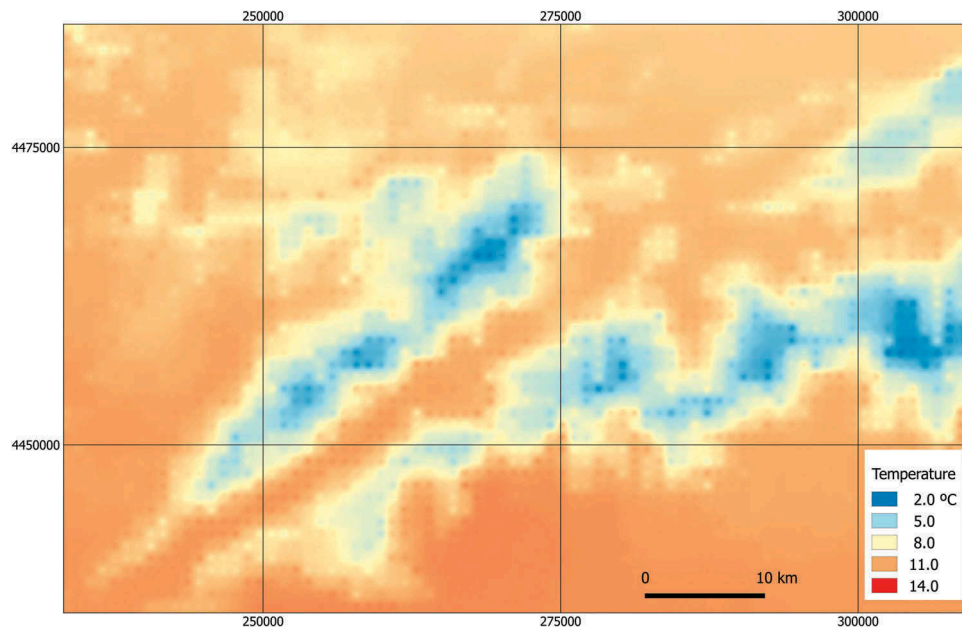

Figure 7. January (day 15) temperature map processed to change the cell size and to make continuous transitions between cells.

each month of the year. Figure 6 shows an example of the index τ corresponding to January (Julian day 15).

Downscaled temperature maps

Twenty-four downscaled temperature maps were calculated using the τ values to modify the original temperature maps. As explained earlier, temperature maps with a cell size of 1 km were converted to 25 m resolution by means of spline interpolation while softening the cell borders, thus making continuous transitions

between source cells. Figure 7 shows an example of this interpolation for the January temperature map (see the original in Figure 4).

Finally, we changed the temperature maps with a cell size of 25 m as a function of τ values. Figure 8 shows the January example for maximum temperatures.

All images with compatible dates (near day 15 of each month) and cloudless conditions (<10% cloud coverage) were downloaded. A set of 5 representative
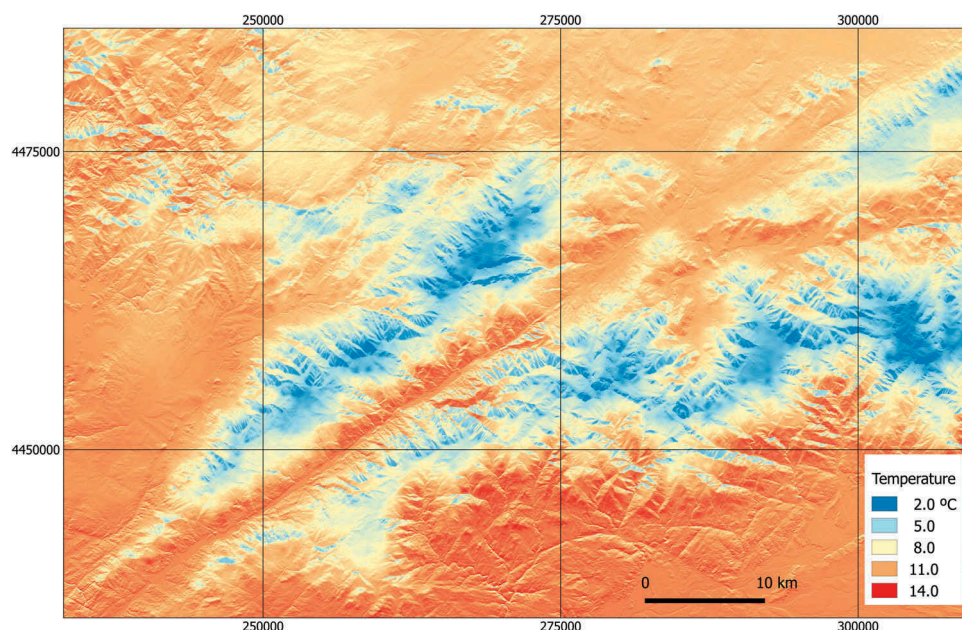
Figure 8. Mean maximum temperature map of January downscaled from a 1 km cell size to 25 m.
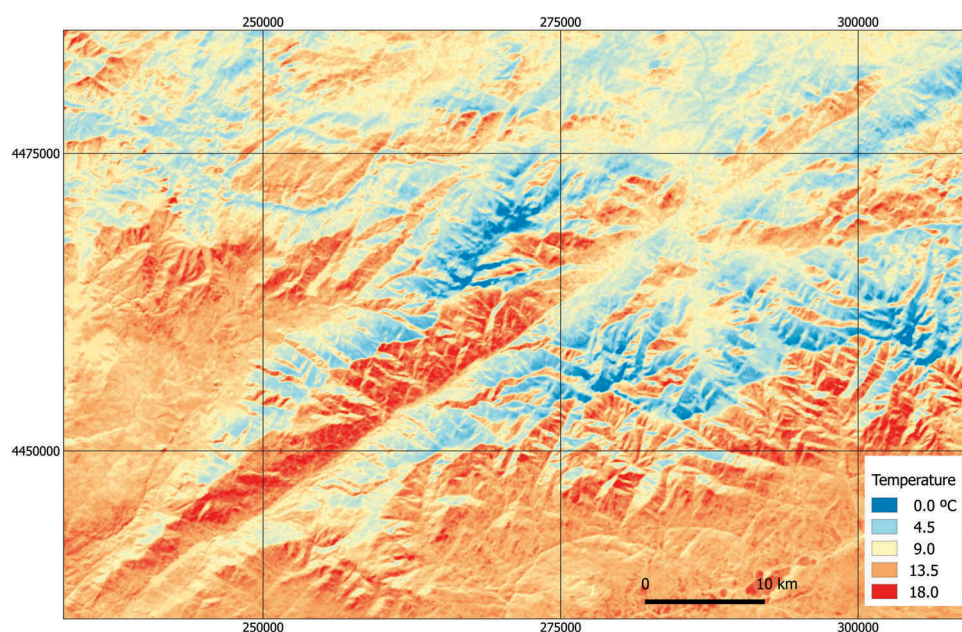

Figure 9. Temperature map derived from thermal imagery (band 10) of the Landsat 8 satellite. Image date: 14 December 2014.

images of the months of July, August, September, October, and December were processed.

From band 10, we calculated surface temperatures by means of the conventional procedure from digital values to top of atmosphere reflectance to at-satellite brightness temperature using the coefficients of the image metadata file. Figure 9 shows the result for the date 14 December 2014.

Table 1 shows the correlation analysis results for the five months with images available. We performed two

series: the first is between the thermal satellite-derived temperatures and the original minimum and maximum temperature maps (r_{ND}), and the second is between the same satellite temperatures and the downscaled minimum and maximum temperature maps (r_{D}). The hypothesis is that if the downscaling procedure is adequate, the correlation will improve significantly.

The result is that all the correlation coefficients increase significantly when the downscaling process is applied, and consequently, the downscaled maps fit

Table 1. Correlation coefficients between satellite thermal-band-derived temperatures and climate maps, without (r_{ND}) and with downscaling (r_D). The increase in correlation coefficients is highly significant.

Month	Julian day	r_{ND}		r_D	
		T_{max}	T_{min}	T_{max}	T_{min}
July	196	.13	.19	.45	.48
August	227	.17	.19	.56	.53
September	257	.19	.21	.67	.68
October	288	.05	.08	.71	.55
December	349	.17	.17	.70	.45

much better with the snapshots captured in the satellite images.

Conclusions and discussion

Temperature maps at moderate or low resolution are commonly available but cannot adequately represent microclimates and fauna or vegetation microrefugia, as they are based on climate estimates that are either too coarse or that ignore relevant topographic climate drivers. This problem worsens in mountainous areas where local contrasts are stronger and meteorological stations are sparse. Downscaling procedures attempt to solve this problem using a variety of methods. This work tested the hypothesis that solar energy and topography are main factors driving local temperature variability. Temperature maps generated by our procedure provide higher resolution than conventional maps. The results give convincing evidence that the downscaling method improves the resolution of temperature maps. A comparison with thermal satellite images shows that the correction strongly increase the correlation (both T_{max} and T_{min}) when the downscaling method is applied to conventional temperature maps (see Table 1). The main advantage is that the method needs only the DEM of the study area and some freely available routines. Additionally, the downscaling takes into account the day of the year and the latitude of the area. However, the main limitation being that the applied Zimmermann or r.sun routines work by default with clear sky conditions. This may be inappropriate even if we are using average values for many years, but it can be adjusted if we have real data on the direct/diffuse radiation ratio in the zone. Additionally, the distribution of temperatures in mountainous terrains depends not only on terrain geometry but also on land cover (forest, rock, pasture, etc.). In our case, this issue can be accommodated because we are working with long-term climate maps. In another case, it may be necessary to classify land cover and assign correction factors.

Overall, our results show that although major limitations remain, climate station data can be used to produce high-resolution temperature maps and, consequently, to model local scale ecological, geomorphological, and soil processes over large areas.

Further studies have already been designed. A wide wireless sensor network (WSN) will be deployed in a mountainous area partially affected by fire, based on a previous article published by the authors (Martín-Tardío & Felicísimo, 2014). This study proposed using temperature as the target environmental variable to achieve: (1) a method to determine the homogeneous environmental classes to be sampled using the DEM and geometric simulations and (2) a procedure to determine an effective WSN design in complex terrain in terms of the number of sensors, redundancy, cost, and spatial distribution. The objective is to measure and monitor *in situ* the spatial and temporal changes in the area over the next several years. Data will be taken hourly, and the results will be compared with satellite images and snapshots taken with a thermal camera to validate this methodology.

ORCID

Á.M. Felicísimo Pérez http://orcid.org/0000-0002-9953-8614
M.Á. Martín-Tardío http://orcid.org/0000-0002-2575-6934

References

Beier, C. M., Signell, S. A., Luttman, A., & DeGaetano, A. T. (2012). High-resolution climate change mapping with gridded historical climate products. *Landscape Ecology*, 27(3), 327–342. doi:10.1007/s10980-011-9698-8

Benestad, R. E., Hanssen-Bauer, I., & Chen, D. (2008). *Empirical-statistical downscaling*. Hackensack, NJ: World Scientific.

Caillouet, L., Vidal, J.-P., Sauquet, E., & Graff, B. (2016). Probabilistic precipitation and temperature downscaling of the twentieth century reanalysis over France. *Climate of the Past*, 12(3), 635–662. doi:10.5194/cp-12-635-2016

Coulibaly, P., Dibike, Y. B., & Anctil, F. (2005). Downscaling precipitation and temperature with temporal neural

networks. *Journal of Hydrometeorology*, 6(4), 483–496. doi:10.1175/JHM409.1

Duhan, D., & Pandey, A. (2015). Statistical downscaling of temperature using three techniques in the Tons River basin in Central India. *Theoretical and Applied Climatology*, 121(3–4), 605–622. doi:10.1007/s00704-014-1253-5

Feidas, H., Karagiannidis, A., Keppas, S., Vaitis, M., Kontos, T., Zanis, P., … Anadranistakis, E. (2014). Modeling and mapping temperature and precipitation climate data in Greece using topographical and geographical parameters. *Theoretical and Applied Climatology*, 118(1–2), 133–146. doi:10.1007/s00704-013-1052-4

Felicísimo, A. M., Muñoz, J., Villalba, C. J., & Mateo, R. G. (2011). *Impactos, vulnerabilidad y adaptación al cambio climático de la biodiversidad española. 1. Flora y vegetación*. Madrid: Ministerio de Medio Ambiente y Medio Rural y Marino. Retrieved from http://www.mapama.gob.es/es/cambio-climatico/temas/impactos-vulnerabilidad-y-adaptacion/lib_imp_cc_flora_tcm7-176082.pdf.

Fridley, J. D. (2009). Downscaling climate over complex terrain: High finescale (<1000 m) spatial variation of near-ground temperatures in a montane forested landscape (Great Smoky Mountains). *Journal of Applied Meteorology and Climatology*, 48(5), 1033–1049. doi:10.1175/2008JAMC2084.1

Gerelchuluun, B., & Ahn, J.-B. (2014). Air temperature distribution over Mongolia using dynamical downscaling and statistical correction: Mongolian temperature reproduction using WRF and a correction method. *International Journal of Climatology*, 34(7), 2464–2476. doi:10.1002/joc.3853

Gerlitz, L. (2015). Using fuzzified regression trees for statistical downscaling and regionalization of near surface temperatures in complex terrain: A case study from Khumbu Himal. *Theoretical and Applied Climatology*, 122(1–2), 337–352. doi:10.1007/s00704-014-1285-x

Hijmans, R. J., Cameron, S. E., Parra, J. L., Jones, P. G., & Jarvis, A. (2005). Very high resolution interpolated climate surfaces for global land areas. *International Journal of Climatology*, 25(15), 1965–1978. doi:10.1002/joc.1276

Kumar, L., Skidmore, A. K., & Knowles, E. (1997). Modelling topographic variation in solar radiation in a GIS environment. *International Journal of Geographical Information Science*, 11(5), 475–497. doi:10.1080/136588197242266

Landgraf, M., Matulla, C., & Haimberger, L. (2015). Statistically downscaled projections of local scale temperature in the topographically complex terrain of Austria up to the end of the 21st century. *Meteorologische Zeitschrift*, 24(4), 425–440. doi:10.1127/metz/2015/0620

Mamassis, N., Efstratiadis, A., & Apostolidou, I.-G. (2012). Topography-adjusted solar radiation indices and their importance in hydrology. *Hydrological Sciences Journal*, 57(4), 756–775. doi:10.1080/02626667.2012.670703

Martín-Tardío, M. A., & Felicísimo, Á. M. (2014). Design of a WSN for the sampling of environmental variability in complex terrain. *Sensors*, 14(11), 21826–21842. doi:10.3390/s141121826

Meineri, E., & Hylander, K. (2016). Fine-grain, large-domain climate models based on climate station and comprehensive topographic information improve microrefugia detection. *Ecography*. doi:10.1111/ecog.02494

Page, J. (1986). *Prediction of solar radiation on inclined surfaces*. Dordrecht: Reidel.

Slavich, E., Warton, D. I., Ashcroft, M. B., Gollan, J. R., & Ramp, D. (2014). Topoclimate versus macroclimate: How does climate mapping methodology affect species distribution models and climate change projections? *Diversity and Distributions*, 20(8), 952–963. doi:10.1111/ddi.12216

Trzaska, S., & Schnarr, E. (2014). *A review of downscaling methods for climate change projections*. Burlington, VT: Tetra Tech ARD for USAID.

USGS. (2016). Using the USGS Landsat 8 Product. Retrieved October 10, 2016, from https://landsat.usgs.gov/using-usgs-landsat-8-product